Pergamon

PII: S0021-8502(00)00049-5

J. Aerosol Sci. Vol. 31, No. 12, pp. 1469–1488, 2000

Printed in Great Britain.
0021-8502/00/$ - see front matter

www.elsevier.com/locate/jaerosci

ON THE RETRIEVAL OF URBAN AEROSOL MASS CONCENTRATION BY A 532 AND 1064 nm LIDAR

Massimo Del Guasta*,† and Stefano Marini‡

*Istituto di Ricerca sulle Onde Elettromagnetiche (IROE) - CNR, Via Panciatichi 64, 50127 Firenze, Italy
†ELIOWATT S.r.l. Via della Pieve in Piano 105, 53034 Colle di val d'Elsa Siena, Italy

(*First received* 11 *October* 1999; *and in final form* 20 *March* 2000)

Abstract—Based on the hypothesis of a monomodal, lognormal size distribution, the uncertainty affecting the humid-mass retrieval from LIDAR data was estimated by considering our ignorance of the distribution width to be a source of error. The mass to backscatter ratio and its uncertainty were computed for six accumulation-mode aerosol models as a function of the backscatter angstrom coefficient (α) and of the relative humidity (RH). A mass to backscatter uncertainty of less than $\pm$ 30% was obtained for all six models. We computed the mass and simulated the expected LIDAR backscatter at 532 and 1064 nm for a test data set of 14 "real-world" multimodal size distributions obtained from the literature. The possible presence of 0–20%–50% water-insoluble compounds in each aerosol mode was assumed. An urban-type accumulation mode and 10 different coarse mode compositions were considered, including dust-like aerosols. The aerosol mass concentration was derived by fitting the simulated LIDAR data at 532 and 1064 nm with a monomodal distribution of urban aerosols of "unknown" width. The relative over- or underestimation of the mass with respect to the real aerosol mass was expressed in terms of α and RH for the 10 coarse aerosol types. The LIDAR-derived mass turned out to be underestimated by 0 – 15% in the case of $(NH_4)_2SO_4$, NaCl, maritime, and H_2SO_4 coarse aerosols. In the case coarse dust aerosols, the range of underestimation was wider (0–30%). Absorbing aerosols showed a maximum underestimation of 40–50%.

1. INTRODUCTION

Fine aerosols in cities are strongly enhanced by combustion. The particles produced by modern engines and heating systems are smaller and less abundant in terms of mass concentration than in the past (Silva and Prather, 1997). Nevertheless, they constitute a danger to health because, mainly in the submicron size, they carry soot, organic compounds and other toxic and carcinogenic substances directly into the lungs (Wilson and Spengler, 1996). The elastic-backscatter LIDAR is a powerful remote-sensing tool that produces vertical, bidimensional, or 3-D qualitative maps of the distribution of aerosols over a city. When used together with ground-based data, this instrument permits a better understanding of the local dynamics of the urban planetary boundary layer (PBL) by considering aerosols as "tracers" of atmospheric motions and/or pollution sources. The possibility of obtaining quantitative information about the PBL aerosol from single-wavelength LIDARs has been explored in recent decades (e.g. Kent, 1978). Even if the LIDAR spatial and temporal resolutions are much larger than the resolution of most *in-situ* instruments, the precision and accuracy of the aerosol information derived are usually much lower than in the case of *in-situ* measurements. This fact is due to the strong variability of PBL aerosol composition and size distributions, which makes it difficult to define a general model for the optical properties of the aerosols. During the last decade, the introduction of multi-wavelength LIDAR has made it possible to improve the accuracy of aerosol measurements (Feingold and Grund, 1994). However, a LIDAR system that could provide a complete size distribution of PBL aerosols has proven so complex (it would require a wavelength range spanning from UV to IR) that it could not be used as a continuous-monitoring tool. Feingold and Grund (1994) pointed out that the use of the LIDAR

† Author to whom correspondence should be addressed.

wavelength pair 532–1064 nm has limited utility for the derivation of aerosol size and concentration in the unpolluted PBL, even in the simple case in which only the accumulation mode is present. The introduction of a coarse aerosol mode in Feingold simulations increased this limitation. This is a big problem, because Nd–YAG lasers that simultaneously produce 532 and 1064 nm are among the most popular, inexpensive and reliable LIDAR sources. In the modern urban environment, fine aerosols are strongly enhanced by combustion (Silva and Prather, 1997), and the use of a 532–1064 nm LIDAR could once again seem attractive — at least for the derivation of bulk quantities such as aerosol mass concentrations.

In this paper, an elastic backscattering LIDAR operating at 532 and 1064 nm is explored as a tool for determining the aerosol mass concentration in an urban environment. The variability of the aerosol modes and composition in this study is considered to be a source of mass uncertainty and, thus, as a loss of information: this approach is similar to the one used by Kent (1978) for a 1064 nm LIDAR. The mass concentration and its uncertainty were derived as a function of the relative humidity (RH) and the LIDAR backscatter at 532 and 1064 nm by assuming a wide variety of aerosol compositions and monomodal size distributions. The introduction of a correction factor (function of RH and of the Angstrom coefficient) made it possible to use the results which are valid for monomodal distributions also in the case of actual multimodal aerosol distributions.

2. MODELING THE URBAN AEROSOL SIZE DISTRIBUTION

PBL aerosols show a complex and very variable number size distribution (SD), the shape of which is often modeled as the sum of three lognormal modes, following the indications of the World Climate Programme, WCP-55 (1983). Each lognormal mode is defined by a total number concentration, N_{ti}, a median radius, r_{mi}, and a geometrical width s_i:

$$n(r) = \frac{dN_i(r)}{dr} = \sum_{i=1}^{3} \frac{N_{ti}}{r \ln(s_i)\sqrt{2\Pi}} \exp\left[-\frac{\ln^2 r/r_{mi}}{2\ln^2 s_i} \right]. \quad (1)$$

The three aerosol modes correspond to Aitken nuclei, accumulation mode aerosols, and coarse aerosols (Whitby, 1977). LIDAR systems operating at 532–1064 nm are practically insensitive to the Aitken mode. For this reason, Aitken particles will be disregarded, in the rest of this study. The PBL aerosol distribution has often been described by means of two modes (Shettle and Fenn, 1979) for optical calculations. Some recent studies (John *et al.*, 1990) have pointed out the presence of a bimodal "accumulation" mode. In these cases, three modes are necessary for modeling the aerosol SD for LIDAR purposes.

In this work, a data set of urban SD obtained from the literature (Table 1) was used for the simulation of LIDAR returns. The data set includes the urban aerosol model of Shettle and Fenn (1979), two averaged distributions (Whitby, 1977), nine real distributions obtained in Vienna with a cascade impactor (Berner *et al.*, 1996), and two mean distributions obtained with impactors in the Los Angeles area by John *et al.* (1990). All the original distributions were converted to numerical distributions. Lognormal volume distributions of median radius r_{mv} were converted to numerical SD by using the relation $r_{mv} = r_m \exp(3 \ln^2 s)$. Aerodynamic equivalent diameters were converted to geometric radii by using a bulk density of 1.6 for the dry particles [all the numerical distributions of Table 1 can be considered to be "dry" aerosol distributions (RH < 50%)]. The estimated ratio between PM2.5 and PM10 was computed for all SD. The no. 4 and 14 distributions, in which the coarse aerosols are relatively more important than in the other SD, are probably representative SD for most towns: the computed ratio PM2.5/PM10 for these SD is, in fact, much lower than 0.8, as observed in the Canadian NAPS network data (Brook *et al.*, 1997) and in most North American urban areas (Schichtel *et al.*, 1999). It must be finally stressed that the results of the present paper are insensitive to any scaling of N_{ti} that would respect the relative importance of the different modes.

Table 1. Aerosol SD derived from data in the literature

No.	Data source	Accumulation modes*						Coarse mode			PM2.5/ PM10
		N_{t1} part cm^{-3}	r_{m1} (μm)	s_1	N_{t2} part cm^{-3}	R_{m2} (μm)	s_2	N_{t3} part cm^{-3}	r_{m3} (μm)	s_3	
1	Shettle and Fenn (1979)				9.9e + 3	3.00e − 2	1.4	1.25	5.0e − 1	1.5	0.87
2	Whitby (1977)				3.2e + 4	2.70e − 2	2.16	5.4	4.3e − 1	2.2	0.89
3	Whitby (1977)				3.7e + 4	3.10e − 2	1.98	4.9	1.1	1.74	0.73
4	Berner *et al.* (1996)				3.1e + 3	6.72e − 2	1.79	3.3e + 1	1.9e − 1	1.93	0.62
5	Berner *et al.* (1996)				1.4e + 3	7.03e − 2	1.72	6.8	3.1e − 1	1.93	0.76
6	Berner *et al.* (1996)				6.7e + 2	9.19e − 2	1.53	7.1	3.1e − 1	1.93	0.93
7	Berner *et al.* (1996)				6.6e + 2	7.23e − 2	1.68	4.4	3.1e − 1	1.85	0.86
8	Berner *et al.* (1996)				1.1e + 3	7.86e − 2	1.62	1.4	3.7e − 1	1.77	0.99
9	Berner *et al.* (1996)				6.5e + 2	8.68e − 2	1.5	2.6	4.3e − 1	1.65	0.94
10	Berner *et al.* (1996)				3.6e + 3	7.08e − 2	1.74	9.0e − 1	6.9e − 1	1.41	0.94
11	Berner *et al.* (1996)				3.4e + 3	7.58e − 2	1.68	1.8e + 2	1.0e − 1	2.0	0.77
12	Berner *et al.* (1996)				5.4e + 2	7.23e − 2	1.54	1.3	2.8e − 1	1.93	0.92
13	John *et al.* (1990)	1.7E4	4.98e − 2	1.5	7.4e + 2	1.18e − 1	1.7	2.7	5.0e − 1	1.9	0.71
14	John *et al.* (1990)	2.6E4	4.98e − 2	1.5	2.0e + 3	8.04e − 2	1.9	3.9e − 1	7.7e − 1	1.8	0.55

*The accumulation mode has been split into two modes for the data of John *et al.* (1990).

3. MODELING THE AEROSOL COMPOSITION

The Aitken and accumulation modes in urban areas are strongly enhanced by direct car emissions (Whitby, 1977; Li *et al.*, 1997; Silva and Prather, 1997). These modes are soot and organic compound-rich (Berner *et al.*, 1996, Brook and Dann, 1999). Accumulation modes were rich in SO_4^{2-}, NH_4^+, and NO_3^- ions in the Los Angeles area (John *et al.*, 1990). SO_4^{2-}, NH_4^+, made up 59% of the accumulation mode mass in the urban plumes observed by Li *et al.* (1997), seemingly in the form of sulfuric acid and ammonium sulfate solutions. $(NH_4)_2SO_4$ and $(NH_4)NO_3$ made up 34% of the mass of particles with an aerodynamic equivalent radius smaller than 1.2 μm in Denver (Sloane, 1983). The rest of the mass consisted of elemental carbon, organic carbon and water. Similar results were obtained in urban areas by the Canadian NAPS network (Brook *et al.*, 1997).

The coarse aerosol mode is rich in dust in urban and rural areas. Sea-salt ions are the most important constituent of coarse aerosols in coastal areas and also in continental, urban areas when synoptic conditions bring in airmasses rich in marine aerosols inland.

Several works (Sloane, 1984; Tang *et al.*, 1981) have suggested that scattering simulations are performed better on externally mixed aerosols than on internally mixed ones. Opposite conclusions were drawn by Sloane (1983) and Sloane and Wolff (1985). McMurry *et al.* (1996) found that the light scattering measured by an integrating nephelometer for fine particles ($r < 1$ μm) in Los Angeles was in good agreement with the Mie simulation, regardless of the model used for the aerosol mixing (internal, external, or hybrid model, based on measured mixing characteristics). In this work, we have assumed internally mixed aerosols.

Even if the bulk composition of the PBL aerosols of different origin is known approximately, the fine composition is strongly variable in both time and space. Aerosol models cannot predict aerosol composition with good accuracy, but they can better predict certain optical properties such as the refractive index: a quantity which drives the light scattering process that is at the basis of the LIDAR. The real part of the aerosol refractive index in the visible spectrum is not very sensitive to chemical composition. The index is variable within the rather limited range of 1.3–1.65 for most aerosol types and RH values. The imaginary part of the index is much more variable, ranging from 1E-9 (e.g. water droplets) to more than 0.1 in very sooty (Shettle and Fenn, 1979) or iron-rich dusty aerosols (Sokolik and Toon, 1999). A small amount of absorbing soot or dust can lead to significant absorption in the particles (Ackermann and Toon, 1981), with serious effects on the LIDAR signals in the urban environment.

The LIDAR measures the light backscattered by the aerosol, that depends on the aerosol complex refractive index and SD. These variables are usually unknown, and the derivation of the aerosol mass from LIDAR data is thus therefore uncertain: it is only possible to simulate the LIDAR return for a wide (and reasonable) range of aerosol types and SD, in order to estimate the uncertainty in the derived mass concentration.

In simulating LIDAR returns, we considered a total of 10 possible bulk compositions for each aerosol mode: the pure (non-absorbing) NaCl, H_2SO_4, and $(NH_4)_2SO_4$ solutions, the urban, rural, and maritime aerosol models of Shettle and Fenn (1979) and, finally four dust-like aerosols. The NaCl solutions are suitable for modeling the thermodynamic and optical properties of coarse aerosols of marine origin (Tang *et al.*, 1997; Tang, 1997). H_2SO_4 may be a dominant compound of fine aerosols, mainly in the vicinity of power plants or industrial areas [the refractive indices of an H_2SO_4 solution and of an HNO_3 solution with the same mass fraction are so close (Pantani, 1996; Luo *et al.*, 1996) that the results obtained in this work for H_2SO_4 are valid in practice also for $H_2SO_4/HNO_3/H_2O$ aerosols]. $(NH_4)_2SO_4$ is one of the most widespread solutes found in fine aerosols.

For NaCl, H_2SO_4, $(NH_4)_2SO_4$ solutions at room temperature, thermodynamic and optical modeling at 532 and 1064 was simple because of the completeness of the data in the literature. The urban model of Shettle and Fenn (1979), that includes about 50% absorbing, soot-like and dust-like substances, was considered suitable for the simulation of urban aerosols, even if the model is based on rather old data. The rural and maritime aerosol

models of Shettle and Fenn (1979) were considered for the modeling of urban aerosols during the advection of air from town suburbs or from long distances.

For the modeling of dust-like coarse aerosols we assumed two dust compositions to be considered "extreme" for scattering simulations: a poorly absorbing aggregate of soil-minerals with 99% quartz (or Kaoline) and 1% Hematite, and an absorbing aggregate of 90% quartz (or Kaoline) and 10% Hematite (Sokolik and Toon, 1999). For each dust composition, we considered separately the cases of subspherical and strongly irregular particles. In the four models, dust-like coarse aerosols were considered completely insoluble, with a density of $2.5\,\mathrm{g\,cm^{-3}}$.

4. MODELING THE AEROSOL GROWTH WITH HUMIDITY

As a first step, we simulated a single lognormal mode of completely soluble particles of NaCl, $(NH_4)_2SO_4$ or H_2SO_4. For these compounds, density ρ and activity coefficient a_w of the aqueous solutions are well known from experiments (Tang and Munkelwitz, 1994; Tang, 1996) to be functions of the mass fraction (x) of the solute:

$$\rho = 0.9971 + \sum_{i=1}^{4} A_i x^i, \tag{2}$$

$$a_w = 1.0 + \sum_{i=1}^{4} C_i x^i. \tag{3}$$

Equations (2) and (3) can be inverted (Table 1) in order to express x and ρ as functions of a_w (Table 1):

$$x = \sum_{j=0}^{5} B_j a_w^j, \tag{4}$$

$$\rho = 0.9971 + \sum_{i=1}^{4} A_i \left(\sum_{j=0}^{5} B_j a_w^j \right)^i. \tag{5}$$

The RH validity range of Table 2 is determined by the polynomial fit for H_2SO_4, and by the crystallization point for the two salts. Starting from a dry aerosol and then increasing RH, the particle begins absorbing humidity at the deliquescence point [approx. 75% RH for NaCl, 80% for $(NH_4)_2SO_4$]. By decreasing RH, the growth curve follows equation (5) back down to the crystallization point [40–46% RH for NaCl, 38% for $(NH_4)_2SO_4$]. In most urban areas of temperate regions, RH is usually higher than 50%, and PBL aerosols rarely experience crystallization. In these conditions, equation (5) is valid between the crystallization point and 99% RH. Also, if $(NH_4)_2SO_4$ is present in a mixture with $(NH_4)_2NO_3$, the dry aerosol is hygroscopic well below the $(NH_4)_2SO_4$ deliquescence point (Sloane, 1984, 1986). McMurry and Stolzenburg (1989) found no evidence of efflorescence or deliquescence for $7\% < \mathrm{RH} < 90\%$ in Los Angeles aerosols, suggesting that the RH validity range listed in Table 2 for NaCl and $(NH_4)_2SO_4$ could also be extended to lower RH.

The relation between a_w and RH is, with surface tension γ, water molecular mass M, and particle radius r:

$$\mathrm{RH} = 100 a_w \exp\left(\frac{2\gamma M_w}{\rho R T r}\right). \tag{6}$$

The activity coefficient a_w is equal to 0.01RH% if the Kelvin effect can be overlooked. This possibility plays a crucial role in this work, because the lognormal shape (and width s_i) of each aerosol mode would be preserved when changing RH. With the SD parameters listed in Table 1, our simulations showed that the Kelvin effect can be overlooked in the coarse mode and in the accumulation mode when $s < 1.9$. This effect will be thus disregarded in the rest of this work, as was done in the works of Shettle and Fenn (1979), Tang and Munkelwitz (1994), and Tang (1996).

Table 2. The polynomial coefficients of equations (4) and (5) for the three pure solutions. The expected RH validity range is reported

	H_2SO_4	NaCl	$(NH_4)_2SO_4$
A_1	7.367E − 03	7.410E − 03	5.92E − 03
A_2	− 4.934E − 05	− 3.741E − 05	− 5.04E − 06
A_3	1.754E − 06	2.252E − 06	1.02E − 08
A_4	− 1.104E − 08	− 2.06E − 08	0
B_0	76	170.8	124.99
B_1	− 157.8	− 770.3	− 312.19
B_2	521.1	2071.4	1158.8
B_3	− 1164.3	− 3094.7	− 2605.4
B_4	1241.9	2388.4	2752.1
B_5	− 517	− 765.8	− 1117.7
RH	25–99%	48–99%	40–99%

When a dry, soluble particle of radius r_{m0} and mass m_0 is embedded in a humid environment, its mass and radius growth ratios G_m and G_r are defined in terms of the equilibrium mass fraction of the solute:

$$G_m = \frac{m}{m_0} = \frac{r_m^3}{r_{m0}^3}\frac{\rho}{\rho_0} = \frac{100}{x}, \tag{7}$$

$$G_r = \frac{r_m}{r_{m0}} = \left(\frac{100}{x}\frac{\rho_0}{\rho}\right)^{1/3}. \tag{8}$$

x and ρ can be derived from equations (4) and (5) as functions of RH only. In this way, it was possible to model the growth of NaCl, H_2SO_4, $(NH_4)_2SO_4$ aerosols.

Several studies have pointed out the widespread presence of water-insoluble material in urban aerosols. Because of the presence of soot and OC, most particles in submicron modes were hydrophobic in Vilnius (Lithuania) (Juozaitis *et al.*, 1993), and in Los Angeles (McMurry and Stolzenburg, 1989). Okada (1985), by using electron microscopy techniques, found that up to 40% in number of the particles with radius 0.03–0.35 μm contained insoluble inclusions. McMurry and Stolzenburg (1989) pointed out the presence of 20–40% non hygroscopic aerosol mass in the coarse mode of Los Angeles aerosols. The inorganic, insoluble fraction of the aerosol reduces the aerosol growth with increasing RH. The hydrophobic organic compounds present in fresh aerosols are also capable of reducing the water uptake of urban aerosols (Pradeep *et al.*, 1995). Naming δ the water-insoluble mass fraction of the "dry" aerosol, the corrected mass growth rate for the partially soluble aerosols is

$$G'_m = \delta + (1 - \delta)G_m. \tag{9}$$

A possible addition of 20 and 50% water-insoluble substance was considered for every aerosol model in this study, by assuming that the main effect of the insoluble substance was to slow down particle growth, disregarding the effect of the insoluble substance on the refractive index.

5. MODELING THE OPTICAL PROPERTIES OF URBAN AEROSOLS

To simulate the optical properties of an aqueous solution of NaCl, $(NH_4)_2SO_4$, and H_2SO_4, we disregarded the imaginary part of the refractive index. We used the partial molar refraction approach (Stelson, 1990) to compute the real part of the refractive indices of these three solutions. In this approach, the real part, m, of the complex refractive index

Table 3. Refractive indices of the three pure solutes used for computing R_i

Pure compound	Refractive index (532 nm)	Refractive index (1064 nm)
H_2SO_4 (95.6% in water)	1.433 (Palmer and Williams, 1975)	1.426 (Palmer and Williams, 1975)
NaCl (solid)	1.544 (Tang, 1996)	1.531 (Burckhardt et al., 1984)
$(NH_4)_2SO_4$ (solid)	1.53 (Burckhardt et al., 1984)	1.509 (Toon, 1976)

Table 4. The refractive indices obtained for the three pure solutions

	H_2SO_4		NaCl		$(NH_4)_2SO_4$	
RH%	m_{532}	m_{1064}	m_{532}	m_{1064}	m_{532}	m_{1064}
50	1.392	1.381	1.412	1.395	1.432	1.413
70	1.376	1.366	1.390	1.376	1.412	1.396
80	1.367	1.357	1.378	1.365	1.399	1.385
90	1.353	1.344	1.361	1.350	1.378	1.366
95	1.344	1.336	1.349	1.339	1.361	1.350
98	1.339	1.330	1.340	1.332	1.346	1.337
99	1.337	1.328	1.337	1.328	1.340	1.332

n was computed by using the results of Moelwyn-Hughes (1961).

$$m = \sqrt{\frac{2R + V_{\text{mol}}}{V_{\text{mol}} - R}}, \tag{10}$$

where V_{mol} ($\text{cm}^3\,\text{mol}^{-1}$) is the molar volume, defined by

$$V_{\text{mol}} = \frac{M}{\rho} = \frac{1}{\rho} \sum_i X_i M_i \tag{11}$$

with M_i being the molecular weight of the ith species, X_i its mole fraction, and ρ is the solution density. R, the molar refraction of the solution, was calculated from the partial molar refraction, R_i, of the solvent and solute, by using:

$$R = \sum_i X_i R_i. \tag{12}$$

The partial molar refraction, R_i, of the ionized solute was computed as the sum of the partial ionic molar refraction of all its ions, weighted by their molal concentrations. The R_i values for NH_4^+, SO_4^{2-}, Na^+, and Cl^- at 532 and 1064 nm were derived from the refractive indices of solid NaCl, solid $(NH_4)_2SO_4$, and 95.6% H_2SO_4 (Table 3).

In the case of a single solute, the molar fractions of the solute (X_2) and the solvent (X_1) for equations (11) and (12) were obtained from the mass concentration x of the solute:

$$X_2 = \frac{x/100M_2}{x/100M_2 + (100 - x)/100M_1}, \quad X_1 = 1 - X_2. \tag{13}$$

The refractive indices of NaCl, $(NH_4)_2SO_4$, and H_2SO_4 solutions were computed for RH = 50, 70, 80, 90, 95, 98, and 99% by using equations (10)–(13) coupled with equations (4) and (5) (Table 4). For the urban, rural, and maritime aerosol models, we obtained the imaginary refractive indices from Shettle and Fenn (1979). The complex refractive indices at 532 and 1064 nm for the dust-like aerosol models were obtained from Sokolik and Toon (1999).

6. SIMULATION OF THE LIGHT BACKSCATTER AT 532–1064 nm

In the hypothesis that aerosols could be assimilated with spherical particles, the Mie theory (Van de Hulst, 1957) is usually applied in order to simulate light scattering. Particles

with a large hygroscopic content (NaCl, $(NH_4)_2SO_4$, H_2SO_4, etc.) can be always considered spherical for RH > 70%. This is the case of most aerosols in the accumulation mode (Okada, 1985; Parungo *et al.*, 1994). At lower RH, hygroscopic $(NH_4)_2SO_4$ particles show scattering functions with only negligible deviations from those of a sphere (Perry *et al.*, 1978). McMurry *et al.* (1996) found by means of experiments that fine (<2 μm) aerosols were almost spherical because of water uptake, even at the low RH found in deserts. The use of Mie codes with fine, hygroscopic aerosols is therefore adequate. The Mie theory could be used also when insoluble, spherical inclusions (g.e. soot) are suspended within hygroscopic spherical matrices (g.e. $(NH_4)_2SO_4$ droplets) (Chylek *et al.*, 1995). In these cases, which are very common in the atmosphere (Okada, 1985; Buseck and Posfai, 1999), the Mie theory could be applied by using the equivalent refractive index of the composite sphere obtained from the refractive-index mixing rule of Maxwell Garnett (1904) or Bruggerman (1935). The volume average of the refractive indexes is also an adequate approximation for LIDAR applications.

Fresh particles produced by combustion and dust are usually slightly hygroscopic and very irregular in shape. Nevertheless, Koepke and Hess (1988) found that the difference between the phase functions of spherical and nonspherical absorbing fine aerosols of both urban and continental types is very small for scattering angles in the 15–170° range. Even if these authors did not study the LIDAR-backscatter region, their findings showed that the Mie theory is not inappropriate for modeling light-scattering on irregular urban aerosols in the accumulation mode.

A different matter is the application of Mie theory to urban coarse aerosols: this aerosol mode is often enhanced by the suspension of dust induced by human activities in towns (Brook and Dann, 1999), and consists of irregularly shaped aerosols that cannot be assimilated to spheres in scattering simulations. Simulations carried out by several authors (Koepke and Hess, 1988; Mishchenko *et al.*, 1997) showed that mixtures of irregular dust-like particles generally show a smaller backscatter than that of equivalent spheres. Mishchenko *et al.* (1999) found that the phase function (averaged over a broad range of particle sizes and shapes) of randomly oriented spheroids having a dust-like refractive index is smooth and featureless closely resembling the phase function measured for natural dust. This result is apparently insensitive to the elementary shape of the particles used in the mixture. The above authors showed that the backscatter of slightly absorbing spheroids (with a modal radius larger than 0.4 μm) is about 50% smaller than the backscatter of equivalent spheres in the 532–1064 nm spectral region. The dust backscatter converged on that of spheres when the imaginary part of the refractive index increased from 0.005 to 0.5, or when smaller particles were considered. On the basis of the Mishchenko *et al.* (1999) results, in the present work, we assumed two "extreme" dust shapes: spherical and highly irregular. The backscatter of irregular dust in the 532–1064 nm range was assumed to be 50% of the backscatter computed by means of the Mie theory for the spherical dust. This way, the backscatter by irregular dust was reconnected to a Mie scattering, for the purposes of error evaluation.

We used a Mie code (Del Guasta, 1991) to compute the Mie backscatter efficiency at the wavelength λ ($Q_{b\lambda}$) and extinction efficiency ($Q_{e\lambda}$) (Van de Hulst, 1957) at 532 and 1064 nm for single particles as functions of the radius r. The radius was varied in the $0.001 < r < 20$ μm range, with constant steps of 0.001 μm.

We computed the $Q_{b\lambda}$ and $Q_{e\lambda}$ efficiencies for the different RH values for each of the 10 aerosol models adopted. Results were weighted with a monomodal, lognormal size distribution, thus obtaining the volume backscatter and volume extinction expected from each aerosol mode:

$$\beta_{s\lambda}(r_m, s, \mathrm{RH}, \mathrm{comp}) = \frac{1}{4\pi} \int_{r=0}^{\infty} Q_{b\lambda}(r)\pi r^2 n(r)\,\mathrm{d}r \quad (\mathrm{m}^{-1}\,\mathrm{sr}^{-1}), \tag{14}$$

$$\sigma_{e\lambda}(r_m, s, \mathrm{RH}, \mathrm{comp}) = \frac{1}{4\pi} \int_{r=0}^{\infty} Q_{e\lambda}(r)\pi r^2 n(r)\,\mathrm{d}r \quad (\mathrm{m}^{-1}) \tag{15}$$

("comp" stands for aerosol composition). The Angstrom coefficient α for the backscatter was also computed for each SD:

$$\alpha(r_m, s, \mathrm{RH}, \mathrm{comp}) = \frac{\ln(\beta_{s532}/\beta_{s1064})}{\ln 2}. \tag{16}$$

In these computations, we assumed an unitary total number of particles N_t,

$$N_t = \int_0^\infty n(r)\,dr = 1 \quad (\mathrm{part\ m^{-3}}). \tag{17}$$

The total aerosol mass concentration corresponding to the selected distribution was computed by

$$M(r_m, s, \mathrm{RH}, \mathrm{comp}) = \tfrac{4}{3}\pi\rho(\mathrm{RH})r_m^3 \exp[\tfrac{9}{2}(\ln s)^2] \quad (\mathrm{kg\,m^{-3}}). \tag{18}$$

For LIDAR applications, it is important to know the conversion factor between the observed, volume backscatter and the aerosol mass concentration. For any distribution, we thus computed:

$$\mathrm{CM}_\lambda(r_m, s, \mathrm{RH}, \mathrm{comp}) = M(r_m, s, \mathrm{RH}, \mathrm{comp})/\beta_{s\lambda}(r_m, s, \mathrm{RH}, \mathrm{comp}) \quad (\mathrm{kg\,m\,sr}). \tag{19}$$

A similar factor was computed for the aerosol number concentration:

$$\mathrm{CN}_\lambda(r_m, s, \mathrm{RH}, \mathrm{comp}) = 1/\beta_{s\lambda}(r_m, s, \mathrm{RH}, \mathrm{comp}) \quad (\mathrm{m\,sr}). \tag{20}$$

Simulations were repeated using a wide range of lognormal parameters: r_m was step-varied between 0.02 and 1 μm with an exponentially spaced step:

$$dr_m(\mu\mathrm{m}) = 0.05 \exp\left[0.025\left(\frac{r_m}{0.05} - 1\right)\right]. \tag{21}$$

According to the s-range of Table 1, s was step varied between 1.4 and 2 with a constant step of 0.02. The backscatter expected from a SD composed of several lognormal modes of different composition was modeled just by adding up the backscatters computed separately for each mode.

7. THE LIDAR DERIVATION OF AEROSOL MASS CONCENTRATION

In principle, an ideal two-wavelength LIDAR operating at 532 and 1064 nm can provide the range-resolved experimental profiles of the volume-backscatter [$\beta'_{s532}(z)$, $\beta'_{s1064}(z)$ ($\mathrm{m^{-1}\ sr^{-1}}$)] and of the angstrom coefficient $\alpha'(z)$ (Measures, 1988). It is possible to compare the experimental and simulated backscatters at some fixed height in order to retrieve some information on the SD. This process requires a certain knowledge of RH and several hypotheses regarding the aerosol composition and the SD shape. Even in the most favorable cases, no more than two independent pieces of information on the SD can be obtained from a two-wavelength LIDAR.

7.1. *Monomodal size distributions*

It was possible to determine the mode radius and the aerosol number (or mass) concentration by assuming a monomodal SD with a fixed width s. Since s was not known *a priori*, it is reasonable to consider it as uncertain and as varying within the range given in Table 1. This range, with a few exceptions, was $s \in [1.4,2]$. By fixing the aerosol composition and RH, we computed α for $s \in [1.4,2]$ as a function of the mode radius. A sample plot is shown in Fig. 1 for RH = 70% and $(NH_4)_2SO_4$ aerosols.

By numerically inverting Fig. 1 it was possible to derive r_m as a function of α (Fig. 2a). Similarly, it was possible to derive CM_{532}, and CN_{532} as functions of α (Fig. 2b and c). The corresponding results for NaCl and H_2SO_4 were very similar to those of $(NH_4)_2SO_4$. By knowing α from the LIDAR, an ignorance of s introduces an uncertainty in r_m, CM_{532}, and

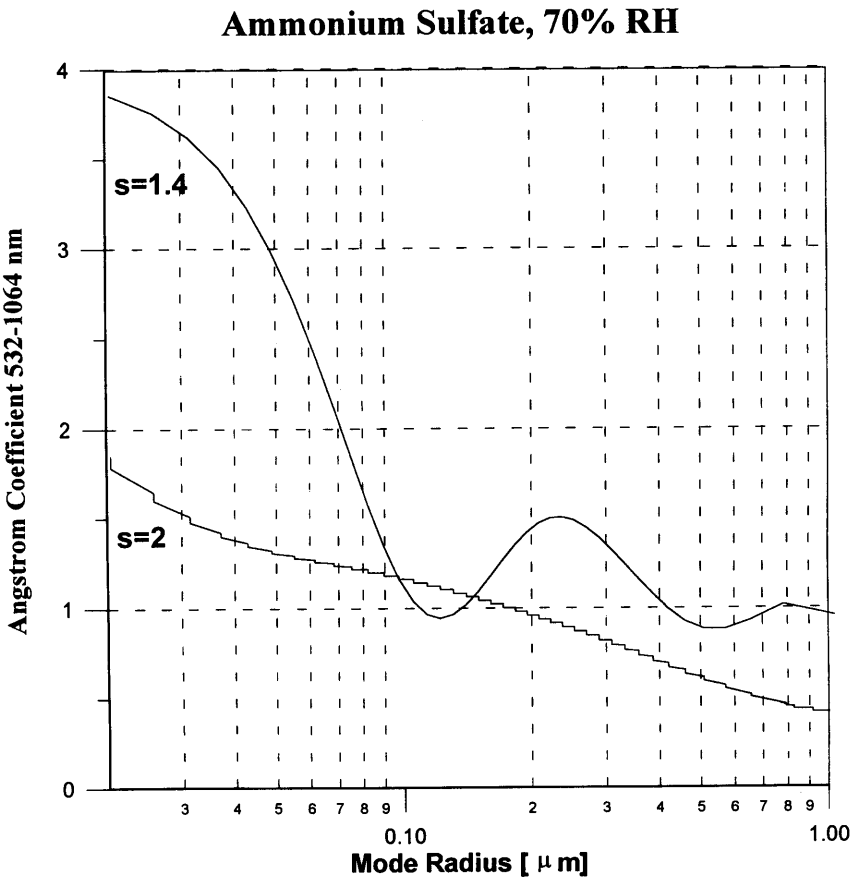

Fig. 1. α values (gray) as obtained for pure $(NH_4)_2SO_4$, 70% RH, $s \in [1.4,2]$. The envelopes of values obtained for $s = 1.4$ and $s = 2$ are marked.

CN_{532}. This uncertainty depends on the "reasonable" range assumed for s, and is an intrinsic uncertainty for this type of LIDAR.

From plots like Fig. 2a–c it was possible to derive numerically the uncertainty for r_m, CM_{532}, and CN_{532} for different RH of the different aerosol models. The results showed that r_m and CN_{532} are affected by great uncertainties, often greater than 100% (Fig. 2a and c). These results support Feingold and Grund (1994), who concluded that N_t and r_m cannot be retrieved unambiguously from 532 to 1064 nm LIDAR measurements. The CM_{532} (and, thus, the aerosol mass) value was the only quantity measurable with some acceptable error. For this reason, the rest of this work will deal with a determination of CM_{532} and related uncertainties.

At a LIDAR site, when RH is known from meteorological probes and α from the LIDAR, it is possible to estimate the minimum and maximum CM_{532} from plots like Fig. 2b, by assuming a model for the dry aerosol. The minimum and maximum mass concentrations can then be derived from these extreme CM_{532} values and from the measured backscatter β'_{532}, by means of equation (19).

In view of this application, CM_{532} max and CM_{532} min were computed as functions of RH and α for the six accumulation mode aerosol models adopted. We computed the "mean" $\langle CM_{532} \rangle$ as $(CM_{532}\text{max} + CM_{532}\text{min})/2$ and the relative "uncertainty" as $(CM_{532}\text{max} - (M_{532}\text{min})/(CM_{532}\text{max} + CM_{532}\text{min})$. It must be stressed that these two quantities are used only to simplify the discussion of the results: they do not have a sound physical meaning since, in the simulations, we implicitly assumed an uniform probability to have distributions with width s in the $s \in [1.4,2]$ range. This hypothesis is unrealistic, so that only the extreme values $CM_\lambda\text{max}$ and $CM_\lambda\text{min}$ have any sound physical meaning.

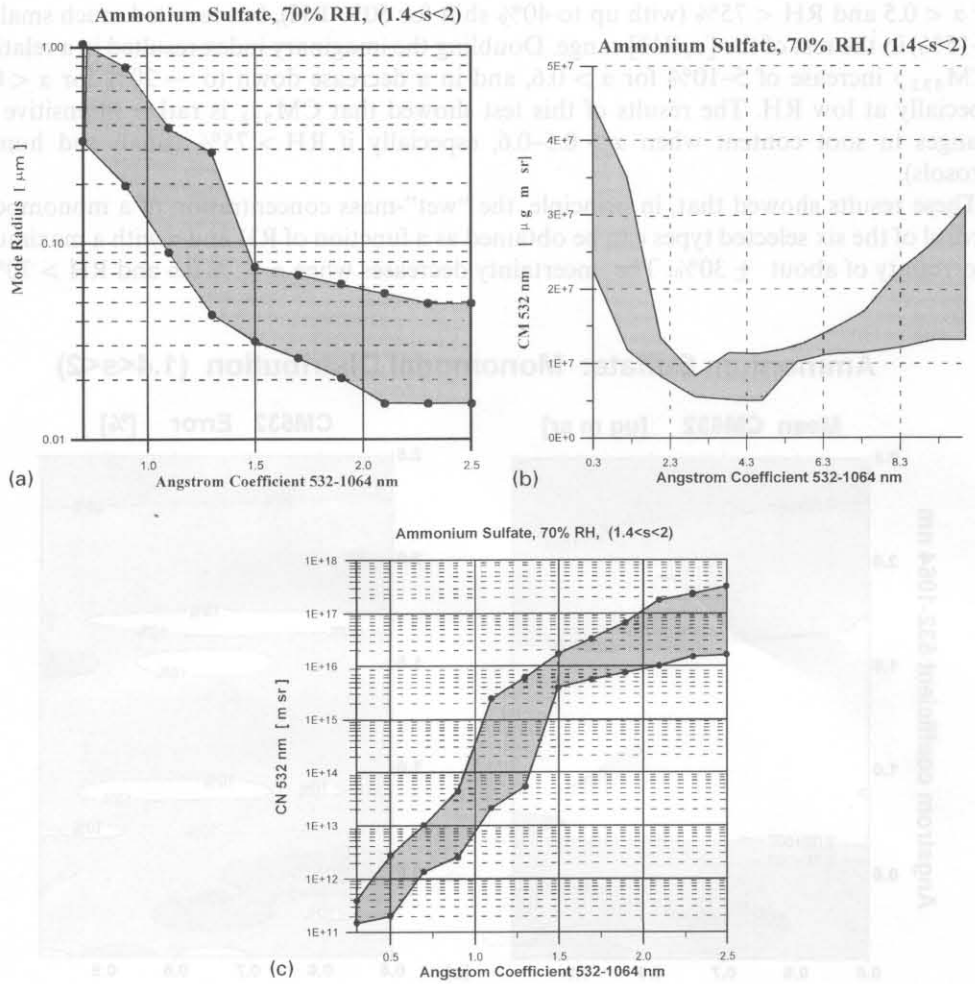

Fig. 2. Mode radius r_m (a); CM_{532} (b), and CN_{532} (c) as functions of α, obtained for pure $(NH_4)_2SO_4$, RH = 70% and $s \in [1.4,2]$.

Results for the six accumulation-mode models are summarized in Fig. 3a–c. Figure 3a shows the results for $(NH_4)_2SO_4$, but is valid also for NaCl, H_2SO_4, and maritime aerosols, since results for these aerosol models are very similar to those of $(NH_4)_2SO_4$ in the same $[\alpha,RH]$ range. Figure 3a shows a flat, $\langle CM_{532} \rangle$ minimum centered around $\alpha = 1$. In this region, CM_{532} uncertainties are about 10–15%. Larger uncertainties, up to 30%, occur with $\alpha < 0.5$ with low RH. Rural aerosols produced a different plot (Fig. 3b), with smaller $\langle CM_{532} \rangle$ values compared with $(NH_4)_2SO_4$, and a slightly larger uncertainty in most of the $[\alpha, RH]$ range, especially at low RH.

Results for urban-type aerosols (Fig. 3c) showed a flat CM_{532} minimum with uncertainties smaller than 15% for $1 < \alpha < 2$. Uncertainties grew up to 30–40% for RH < 75% and $\alpha < 0.7$, but were smaller than 25% for RH > 75%. The soot content of urban aerosols varies both in time and space, and so does the imaginary part of the refractive index. The presence of considerable absorption makes a marked difference between Fig. 3c and a, since the real part of the refractive indices are rather similar in all the models adopted. A test was carried out in order to assess the sensitivity of the LIDAR simulations to a change in the urban-aerosol imaginary index: starting from the urban model of Shettle and Fenn (1979), we repeated the simulations by decreasing the imaginary part of the refractive index by a factor 0.5, and by increasing it by a factor 2. Results are shown in Fig. 4a and b in terms of $\langle CM_{532} \rangle$ relative shift with respect to the original urban model. The reduced absorption resulted in a decrease in $\langle CM_{532} \rangle$ over the whole $[\alpha, RH]$ range. The shift was important

for $\alpha < 0.5$ and RH $< 75\%$ (with up to 40% shift for 50% RH), but resulted much smaller (5–15%) in the rest of the [α, RH] range. Doubling the imaginary index resulted in a relative $\langle CM_{532} \rangle$ increase of 5–10% for $\alpha > 0.6$, and in a decrease down to -20% for $\alpha < 0.6$ especially at low RH. The results of this test showed that CM_{532} is rather insensitive to changes in soot content when $\alpha > 0.5$–0.6, especially if RH $> 75\%$ (small and humid aerosols).

These results showed that, in principle, the "wet"-mass concentration of a monomodal aerosol of the six selected types can be obtained as a function of RH and α with a maximum uncertainty of about $\pm 30\%$. The uncertainty decreases when $\alpha > \approx 0.6$ and RH $> 70\%$.

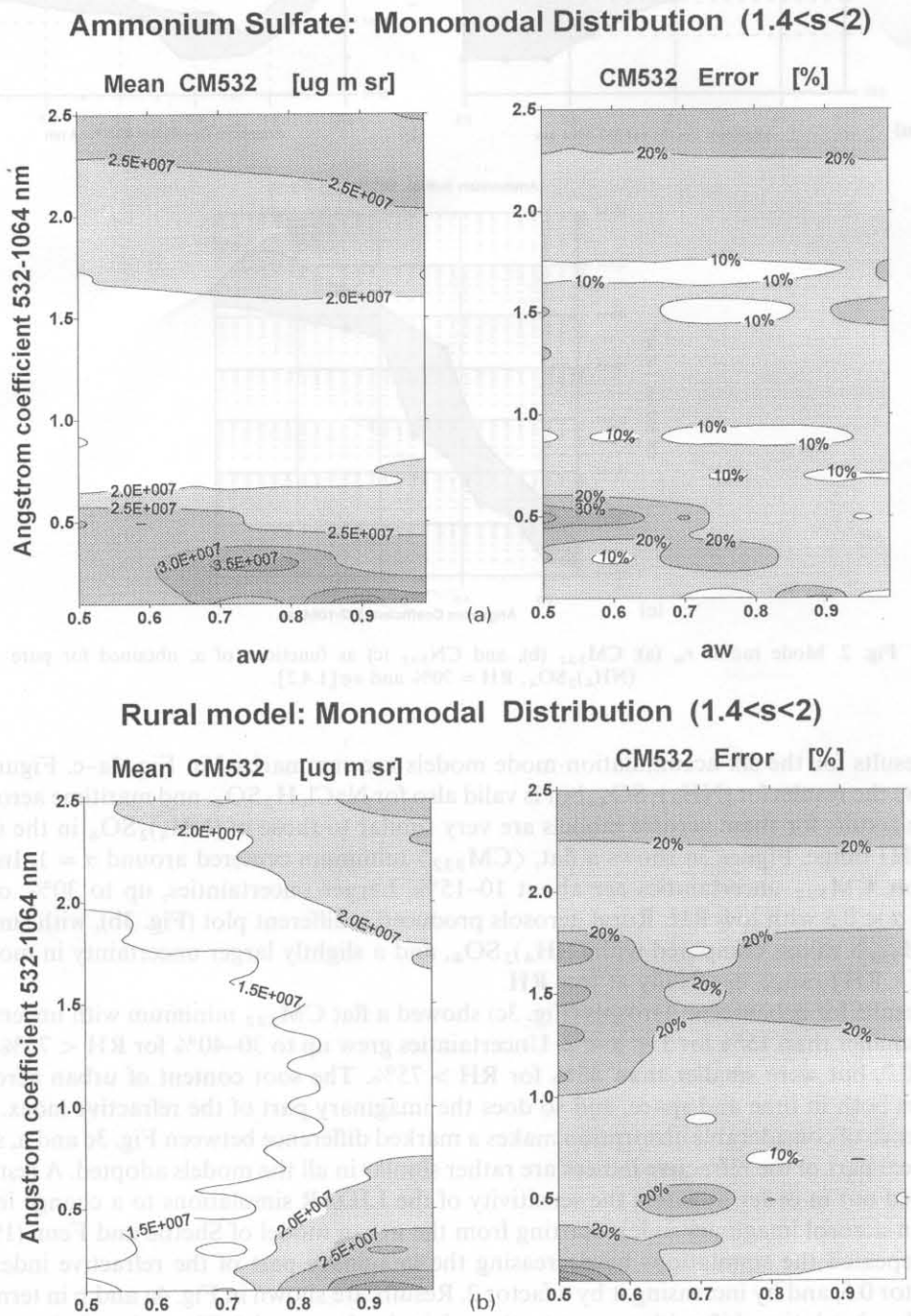

Fig. 3. The "mean" CM_{532} and the relative uncertainty for monomodal SD of fixed composition: (a) $(NH_4)_2SO_4$, NaCl, H_2SO_4; maritime model; (b) rural model; (c) urban.

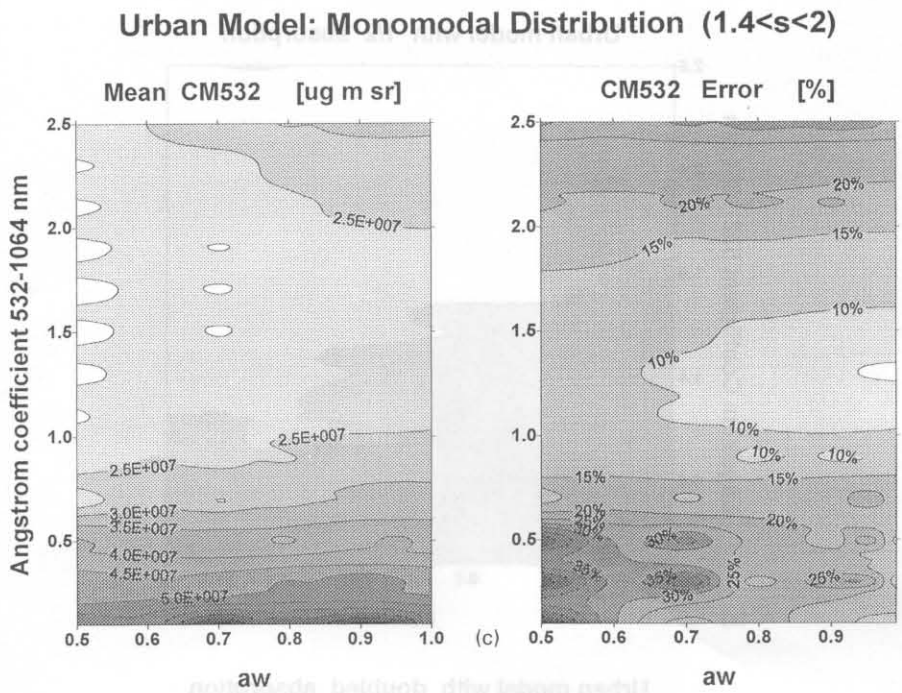

Fig. 3. (*Continued*).

7.2. *Introducing "real-world" multimodal size distributions*

The next step was to consider the additional presence of insoluble substances in all the aerosol models and a multimodal SD that included the coarse mode.

In the case of a real SD, the coarse aerosol mode contributes significantly to the aerosol mass, and cannot be disregarded in a modeling of aerosol scattering. A test to assess the impact of the coarse mode on the LIDAR-derived aerosol mass was performed using the SD of Table 1 as test distributions. Each tabulated distribution was developed up to the equilibrium with RH (equation (8)), by assuming the possible additional presence of insoluble mass in each mode. We computed β_{s532}, β_{s1064}, α, M for the developed multimodal SD by using equations (14), (16), and (18). $PM_{2.5}$ and PM_{10} were also computed. In the simulation, the accumulation mode composition was fixed [urban model of Shettle and Fenn (1979)], and the coarse mode composition was varied among the ten aerosol models adopted. For the SD N.13 and 14, the same aerosol composition was assumed for the two modes describing the "accumulation" aerosol. The presence of 0%, 20%, 50% insoluble mass in the accumulation mode was considered. In the coarse mode, the presence of 0%, 20%, 50% insoluble mass was also considered, with the exception of the four dust-like models, for which a 100% insoluble mass was assumed. A total of 58 backscatter simulations for each of the 14 distributions of Table 1 and for each RH value was thus obtained.

For each simulation, by using the results of Section 7.1, we determined the mass concentration $M_I(r_m, s, \mathrm{RH}, \mathrm{comp})$ of the monomodal SD (urban aerosol model) matching the computed optical quantities β_{s532} and α.

The equivalent M_I was not unique because, in order to determine it, we assumed that s was uncertain. The minimum ($M_{Imin} = \beta'_{s532}\mathrm{CM}_{532min}$) and the maximum masses ($M_{Imax} = \beta'_{s532}\mathrm{CM}_{532max}$) of the equivalent monomodal SD were computed and compared with the original mass M. In this way, the validity of the monomodal approximation in the derivation of aerosol mass from "real-world" LIDAR data could be tested against different coarse aerosol compositions. The ratio

$$\mathrm{CF}(\mathrm{RH}, \alpha) = \frac{M - M_{Imin}}{M_{Imax} - \mathrm{M}_{Imin}} \tag{22}$$

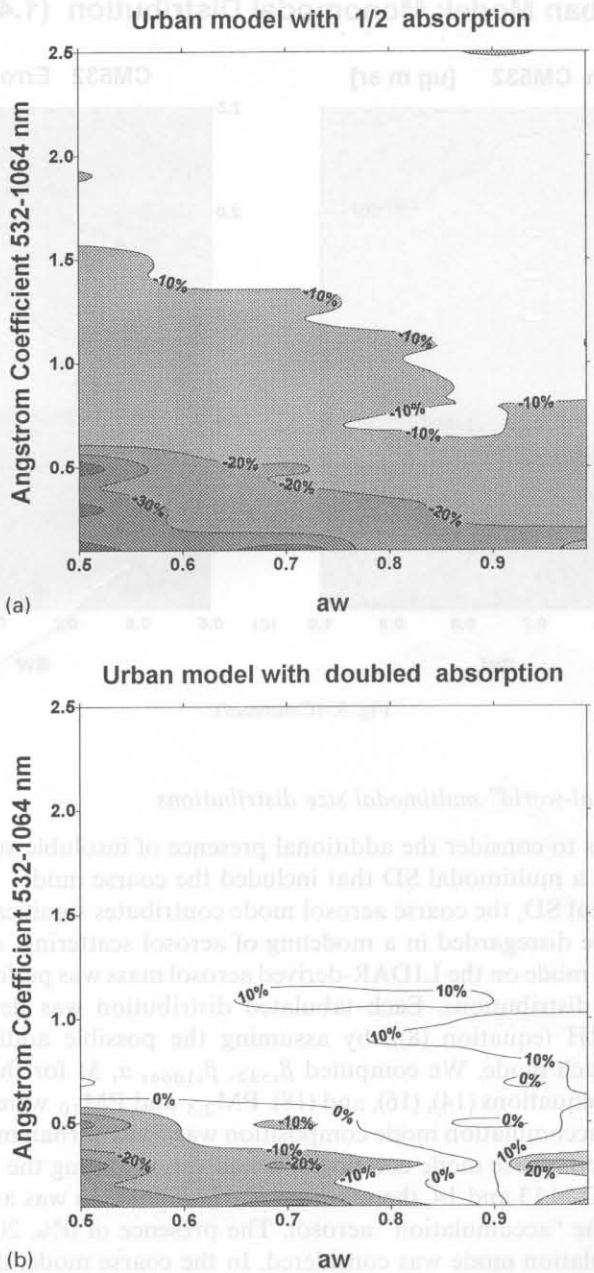

Fig. 4. Relative shift of $\langle CM_{532} \rangle$ for aerosols of urban type after (a) reduction of the imaginary part of refractive index to 1/2 of the original value; (b) doubling of the imaginary part of the refractive index.

is in the [0,1] range if the aerosol mass M is within the $[M_{\mathrm{Imin}}, M_{\mathrm{Imax}}]$ mass uncertainty range obtained by inverting the LIDAR data in the hypothesis of a monomodal distribution of urban aerosols. If CF is larger than 1, M is above the $[M_{\mathrm{Imin}}, M_{\mathrm{Imax}}]$ uncertainty range, indicating that the LIDAR-derived mass is underestimated with respect to the real one. A measure of underestimation is, in this case: $\Delta = (M_{\mathrm{Imax}} - M)/M$. If $CF < 0$, a mass overestimation occur, defined by: $\Delta = (M_{\mathrm{Imin}} - M)/M$. Computing Δ for the different test distributions by varying the coarse mode composition and the insoluble content, Fig. 5a–d were obtained. In these plots, only cases with $CF < 0$ and $CF > 1$ are reported, because when $0 < CF < 1$, no mass overestimation or underestimation occurred. Figure 5a–d thus show the extreme Δ values expected when using a monomodal distribution to fit the LIDAR data, and not the most probable values, that are much smaller. In Fig. 5a–d, the

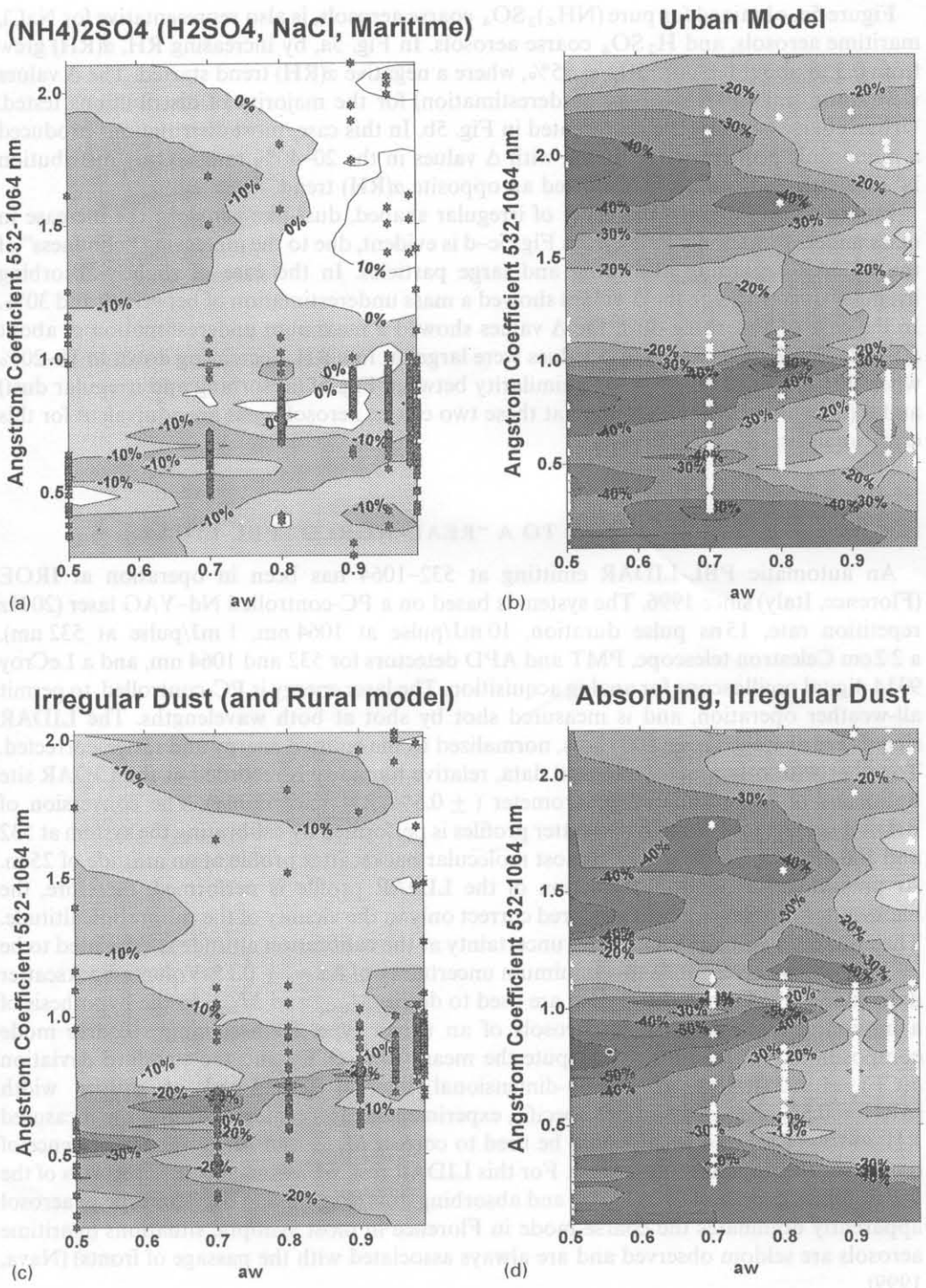

Fig. 5. Extreme values of Δ mass underestimation-overestimation) expected when fitting the LIDAR data with a monomodal (urban model) SD. Δ is due to the presence of coarse aerosols and insoluble substance, and to the uncertainty of *s*. (a) $(NH_4)_2SO_4$, NaCl, H_2SO_4, maritime model; (b) urban model; (c) irregular dust, slightly absorbing, rural model; (d) irregular, absorbing dust. Star-symbols show α(RH) as calculated for the different test SD with different insoluble contents.

(RH,α) points obtained with the different test distributions are also shown. The distribution of (RH,α) points on the graphs show the expected trend of α(RH) for different coarse aerosol types. Compared with LIDAR-derived ones, these trends could be used as diagnostic tools to identify the coarse aerosol type.

Figure 5a, obtained for pure $(NH_4)_2SO_4$ coarse aerosols, is also representative for NaCl, maritime aerosols, and H_2SO_4 coarse aerosols. In Fig. 5a, by increasing RH, α(RH) grew from 0.5 to about 0.8 until RH = 95%, where a negative α(RH) trend started. The Δ values were quite small (0–15% mass underestimation) for the majority of distributions tested. Urban coarse aerosols are represented in Fig. 5b. In this case, most distributions produced a monotonic positive α(RH) trend, with Δ values in the 20–40% range. Only distribution N°1 (Shettle & Fenn model) showed an opposite α(RH) trend.

Figure 5c and d show the effect of irregular shaped, dust-like aerosols: the increase in mass underestimation passing from Fig. 5c–d is evident, due to the increasing "blindness" of the LIDAR regarding absorbing and large particles. In the case of slightly-absorbing irregular dust (Fig. 5c), the Δ values showed a mass underestimation of between 0 and 30%. In the case of absorbing dust, the Δ values showed a maximum underestimation of about 50–60%. In all dust cases, the Δ values were larger at low RH, decreasing down to 10–20% when RH exceeded 80–85%. The similarity between Fig. 5f (absorbing and irregular dust) and b (urban model), suggesting that these two coarse aerosol types are equivalent for this error analysis, must be stressed.

8. APPLICATION TO A "REAL-WORLD" PBL-LIDAR

An automatic PBL-LIDAR emitting at 532–1064 has been in operation at IROE (Florence, Italy) since 1996. The system is based on a PC-controlled Nd–YAG laser (20 Hz repetition rate, 15 ns pulse duration, 10 mJ/pulse at 1064 nm, 1 mJ/pulse at 532 nm), a 2 2 cm Celestron telescope, PMT and APD detectors for 532 and 1064 nm, and a LeCroy 9314 digital oscilloscope for analog acquisition. The laser energy is PC-controlled, to permit all-weather operation, and is measured shot by shot at both wavelengths. The LIDAR signals are averaged over 500 shots, normalized to the emitted energy and range-corrected. Together with other meteorological data, relative humidity is recorded at the LIDAR site by means of an automated psycrometer ($\pm$ 0.5% RH uncertainty). The conversion of LIDAR signals to volume-backscatter profiles is performed by calibrating the system at 532 and 1064 nm with a clear-day, almost molecular backscatter profile at an altitude of 25 m. At present, no extinction correction of the LIDAR profile is performed; therefore, the backscatter profiles can be considered correct only in the vicinity of the calibration altitude. The minimum volume-backscatter uncertainty at the calibration altitude is estimated to be $\pm$ 5%, which corresponds to a minimum uncertainty of $\Delta\alpha = \pm 0.15$. Volume-backscatter data at 532–1064 nm and RH data are used to derive M_{Imin} and M_{Imax} in the hypothesis of a monomodal distribution of aerosols of an urban type. By assuming a coarse mode composition, it is possible to compute the mean value $\langle \mathrm{CF} \rangle$ and the standard deviation σ(CF) of CF(RH, α) in a two-dimensional interval [ΔRH, $\Delta\alpha$] of proper width (ΔRH = 0.5%, $\Delta\alpha = 0.28$ in this specific, experimental case) centered around the measured RH and α. $\langle \mathrm{CF} \rangle$ and σ(CF) could be used to correct M_{Imin} and M_{Imax} for the presence of coarse aerosols and insoluble mass. For this LIDAR test, we assumed coarse aerosols of the urban type (equivalent to irregular and absorbing dust (Fig. 5b and d)). This type of aerosol apparently dominates the coarse mode in Florence in most synoptic situations (maritime aerosols are seldom observed and are always associated with the passage of fronts) (Nava, 1999).

Using the scattering simulations described in this work, software has been developed for processing LIDAR data automatically in terms of aerosol mass concentration. [RH, α] pairs are fitted with a monomodal, lognormal distribution of urban-type aerosols to give the $[M_{\mathrm{Imin}}, M_{\mathrm{Imax}}]$ range. A possible correction for this mass-range, accounting for the presence of coarse aerosols and insoluble mass, is $[M'_{\mathrm{Imin}}, M'_{\mathrm{Imax}}]$:

$$M'_{\mathrm{Imin}} = (\langle \mathrm{CF} \rangle - 0.5)(M_{\mathrm{Imax}} - M_{\mathrm{Imin}}) + M_{\mathrm{Imin}},$$

$$M'_{\mathrm{Imax}} = (\langle \mathrm{CF} \rangle + 0.5)(M_{\mathrm{Imax}} - M_{\mathrm{Imin}}) + M_{\mathrm{Imin}}.$$

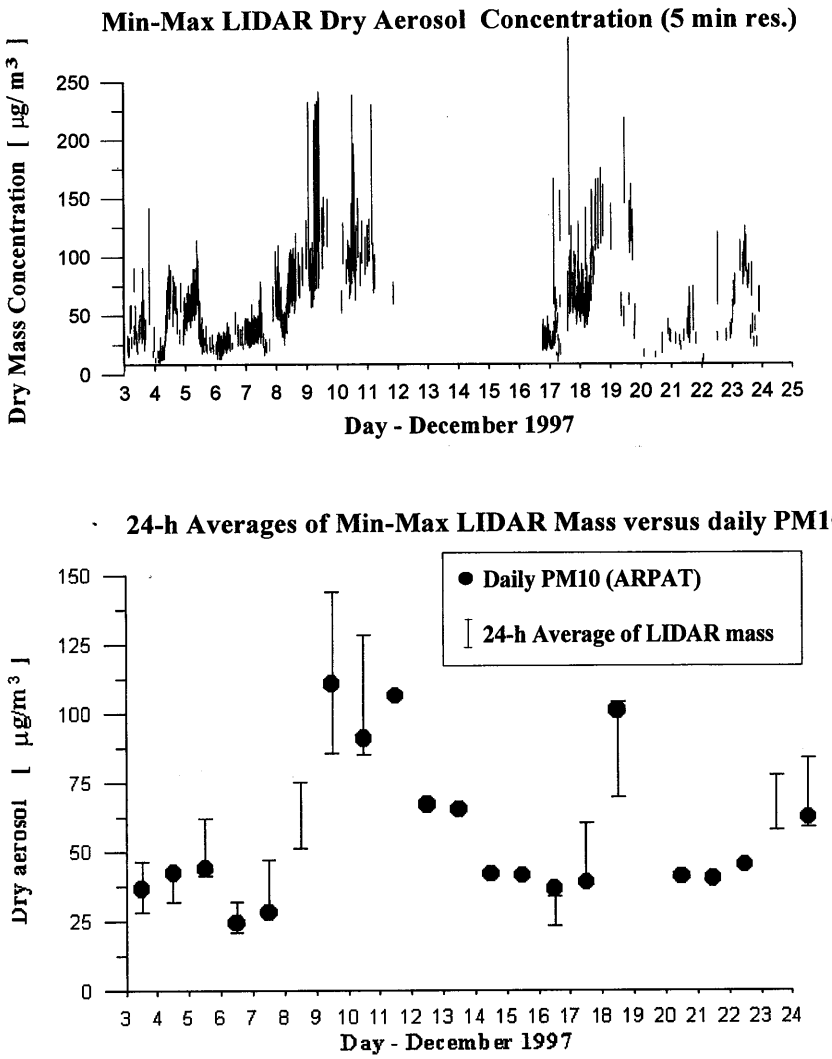

Fig. 6. (a) $[M'_{I\min}\ M'_{I\max}]$ (see text) obtained from 532–1064 nm LIDAR data with 5 min resolution. (b) Twenty-four-hour averages of LIDAR-derived, dry aerosol, min–max mass concentrations compared with the daily PM10 data (ARPAT).

This type of correction shifts the original $[M_{I\min}, M_{I\max}]$ range upward, in order to cancel the expected mass under-overestimation. The validity of this process is closely connected to the local significance of the test distribution data set used to obtain the correction factor CF.

A sample of the results is shown in Fig. 6. Data refer to December 1997, and include two pollution episodes (9–12 and 18–19 December). Figure 6a shows the LIDAR-derived mass range $[M'_{I\min}, M'_{I\max}]$, when available and validated, obtained with 5 min resolution at an altitude of 25 m. The high variability of the LIDAR-derived mass, due partly to the wide time variability of the aerosol concentration, and partly to the rather large mass uncertainties discussed in this work, is evident. Greater uncertainties occurred with RH < 50% (on 7 and 8 December), or in cases of fog formation (18 December).

In Fig. 6b we perform a comparison between the 24-h averages of $[M'_{I\min}, M'_{I\max}]$ and ground-based daily PM_{10} pollution data, measured by using a standard filtering technique from the "Agenzia Regionale per la Protezione Ambientale della Toscana (ARPAT)" in a street located 1000 m from the LIDAR site. Since PM_{10} is a measurement of dry aerosol mass, while LIDAR-derived masses are "wet" masses, $M'_{I\min}$ and $M'_{I\max}$ were converted to dry masses by arbitrarily considering a 20% insoluble (dry) mass, and the hygroscopic

growth rate of $(NH_4)_2SO_4$. Twenty-four-hour averages of LIDAR data were shown only when a minimum of 6 h of daily LIDAR data were available. Despite the errors involved in the overall process and the spatial distance between the two monitoring instruments, LIDAR-derived data showed an encouraging agreement with PM_{10} data.

9. CONCLUSIONS

The advantages of the LIDAR, compared to the usual filtering techniques used for PM monitoring, are its high temporal and spatial resolutions, that makes it possible to obtain a time-altitude-aerosol mass concentration "snapshot" of the PBL aerosol in real time. This advantage is counter-balanced by the intrinsically poor accuracy of the LIDAR in terms of PBL aerosol quantities. In assuming that either calibrated backscatter values at a fixed height or extinction-corrected backscatter profiles could be retrieved, the 1064–532 nm elastic-backscatter LIDAR could be used to determine the urban aerosol mass concentration. This is possible because CM_λ is much less sensitive to aerosol composition and SD than other aerosol quantities (such as r_m and CN_λ) are. But even in the case of ideal, error-free 532–1064 nm LIDAR backscatter data, the aerosol mass uncertainty produced by an ignorance of aerosol properties would be as great as 20–30% or more.

When the accumulation mode dominates the LIDAR signal, the SD can be assimilated to a monomodal distribution. In this case, in choosing a model for dry-aerosol composition, a mass-concentration uncertainty of less than $\pm$ 30% is expected for most (RH, α) pairs. Larger errors are expected for some aerosol models with $\alpha < 0.7$ and RH $< 70\%$. This uncertainty is due to a lack of knowledge regarding the SD width. Since the real part of the aerosol refractive index is relatively insensitive to the fine chemical composition of dry aerosols, it is expected that, for LIDAR purposes, even the most refined microphysical models for urban aerosols would give results similar to those obtained with the simple model of Shettle and Fenn (1979). In support of this hypothesis, the results of this work show that the CM_{532} values derived for six extremely different aerosol models differed by less than 30% for (α, RH) pairs chosen in the $60\% < RH < 99\%$, $0.7 < \alpha < 1.5$ range. The imaginary part of the refractive index, on the other hand, is very sensitive to the presence of small quantities of soot or absorbing particles, and could show a wide temporal and spatial variability in the urban environment. A sensitivity test performed by varying the imaginary part of the refractive index of urban aerosols showed that CM_{532} values are quite insensitive to absorption variations if $\alpha > 0.5$ and RH $> 70\%$.

When coarse aerosols are expected to contribute significantly to the LIDAR signal, and water-insoluble particles are assumed to be present in each mode with an unknown mass concentration, it is still possible to use a monomodal SD of urban-type aerosols to fit the LIDAR backscatter data. In this case, however, the mass uncertainty grows. The test performed on the SD data set of Table 1 showed that, when the coarse mode was disregarded, mass underestimation prevailed, with an expected underestimation from 0 to 10% (in the case of $(NH_4)_2SO_4$, NaCl, maritime, and H_2SO_4 aerosols) up to 30–40% for absorbing aerosols such as urban and absorbing, irregular, dust particles.

A correction factor (depending on RH and α) can be used to compensate the mass underestimation induced by coarse aerosols. This factor, whose numerical values must be confirmed locally on the basis of a true SD statistic, makes it possible to use a monomodal fit of the 532–1064 nm LIDAR data for estimating the suspended mass, in the absence of real time, *in-situ* information on the aerosol SD and optical properties. In cases in which strongly absorbing coarse aerosols are present (such as soot-rich urban aerosols or absorbing, irregular dust), the correction factor could be dangerously large (up to 1.5). This situation could occur either during the advection of Saharian dust in the Mediterranean region or in soot-polluted towns. In all these cases, some ancillary, real-time information about the coarse mode magnitude and composition should be derived with *in-situ* instruments, in order to improve the poor accuracy of the LIDAR technique. LIDAR depolarization can also be used to state the presence of coarse, dust-like aerosols.

Acknowledgements—We are grateful to the "Agenzia Regionale per la Protezione Ambientale della Toscana (ARPAT)" for the pollution data used in this paper. We thank Stefano Balestri, Francesco Castagnoli, Marco Morandi, and Valerio Venturi for the design and implementation of the PBL-LIDAR.

REFERENCES

Ackermann, T. P. and Toon, O. B. (1981) Absorption of visible radiation in atmospheres containing mixtures of absorbing and nonabsorbing particles. *Appl. Opt.* **20,** 3661–3667.

Berner, A., Sidla, S., Galambos, Z., Kruisz, C., Hitzenberger, R., ten Brink, H. M. and Kos, G. P. A. (1996) Modal character of atmospheric black carbon size distributions. *J. Geophys. Res.* **101**(D14), 19,559–19,565.

Brook, J. R., Dann, T. F. and Burnett, R. T. (1997) The relationships among TSP, PM10, PM2.5, and inorganic constituents of atmospheric particulate matter at multiple Canadian locations. *J. Air Waste Manage. Assoc.* **47,** 2–19.

Brook, J. R. and Dann, T. F. (1999) Contribution of nitrate and carbonaceous species to PM2.5 observed in Canadian cities. *J. Air Waste Manage. Assoc.* **49,** 193–199.

Bruggerman, C. A. G. (1935) Berechnung verschiedener physikalischer konstanten von heterogenen subsganzen. *Ann. Phys. Leipzig* **24,** 636–649.

Burckhardt, W., *et al.* (1984) Structure and molar refraction and its wavelength dependence at different alkali and ammonium halides. *J. Phys. Stat. Sol. A* **85**(1), 97–103.

Buseck, P. R. and Posfai, M. (1999) Airborne minerals and related aerosol particles: effects on climate and the environment. *Proc. Natl. Acad. Sci. U.S.A. (PNAS)* **96**(7), 3372–3379.

Chylek, P., Videen, G., Ngo, D. and Pinnick, R. G. (1995) Effect of black carbon on the optical properties and climate forcing of sulfate aerosols. *J. Geophys. Res.* **100**(D8), 16,325–16,332.

Del Guasta, M. (1991). Programma FORTRAN per il calcolo rapido dello scattering da particelle sferiche, con particolare applicazione al backscattering LIDAR. Report IROE TR/GCF/01.22, pp. 20.

Feingold, G. and Grund, C. G. (1994) Feasibility of using multiwavelength LIDAR measurements to measure cloud condensation nuclei. *J. Atmos. Oceanic Technol.* **11,** 1543–1558.

John, W., Wall, S. M., Ondo, J. L. and Winklmayr, W. (1990) Modes in the size distributions of atmospheric inorganic aerosols. *Atmos. Environ.* **24A**(9), 2349–2359.

Juozaitis, A., Ulevicius, V. and Girgzdys, A. (1993) Differentiation of hydrophobic from hydrophilic submicrometer aerosol particles. *Aerosol Sci. Technol.* **18,** 202–212.

Kent, G. S. (1978) Deduction of aerosol concentrations from 1.06-μm lidar measurements. *Appl. Opt.* **12**(23), 3763–3773.

Koepke, P. and Hess, M. (1988) Scattering functions of tropospheric aerosols: the effect of nonspherical particles. *Appl. Opt.* **27**(12), 2422–2430.

Li, S.-M., Macdonald, A. M., Strapp, J. W., Lee, Y.-N. and Zhou, X.-L. (1997) Chemical and physical characterization of atmospheric aerosols over southern California. *J. Geophys. Res.* **102**(D17), 21,341–21,353.

Luo, B., Krieger, U. K. and Peter, T. (1996) Densities and refractive indices of $H_2SO_4/HNO_3/H_2O$ solutions to stratospheric temperatures. *Geophys. Res. Lett.* **23**(25), 3707–3710.

Maxwell Garnett, J. C. (1904) Colours in metal glasses and in metallic films. *Philos. Trans. Roy. Soc. London* **203,** 385–395.

McMurry, P. H. and Stolzenburg, M. (1989) On the sensitivity of particle size to relative humidity for Los Angeles aerosols. *Atmos. Environ.* **23**(2), 497–507.

McMurry, P. H., Zhang, X. and Lee, C. (1996) Issues in aerosol measurement for optics assessment. *J. Geophys. Res.* **101**(D14), 19,189–19,197.

Measures, R.M. (1988). Laser Remote Chemical Analysis, pp. 49. Wiley, New York.

Mishchenko, M. I., Travis, L. D., Kahn, R. A. and West, R. A. (1997) Modeling phase functions for dustlike tropospheric aerosols using a shape mixture of randomly oriented polydisperse spheroids. *J. Geophys. Res.* **102**(D14), 16,831–16,847.

Moelwyn-Hughes, E.A. (1961). Physical Chemistry, 2nd revision, pp. 420. Pergamon Tarrytown, New York.

Nava, S. (1999). Inquinamento atmosferico nell'area fiorentina: uno studio dell'andamento stagionale della composizione dell'aerosol tramite analisi con fasci ionici. Universita' degli Studi di Firenze, Fac. Sci. Mat. Fis. Nat., 1989–1999, p. 130.

Okada, K. (1985) Number-size distribution and formation process of submicrometer sulfate-containing particles in the urban atmosphere of Nagoya. *Atmos. Environ.* **19**(5), 743–757.

Palmer, K. F. and Williams, D. (1975) Optical constants of sulfuric acid: application to the clouds of Venus?. *Appl. Opt.* **14**(N1), 208–219.

Pantani, M. (1996). Studio di nubi polari stratosferiche mediante lidar multispettrale. Thesis, Universita' degli studi di Firenze, Facolta' Sci. Mat. Fis. Nat., p. 106.

Parungo, F., Nagamoto, C., Zhou, M. Y., Hansen, A. D. A. and Harris, J. (1994) Aeolian transport of aerosol black carbon from China to the Ocean. *Atmos. Environ.* **28**(20), 3251–3260.

Perry, R. J., Hunt, A. J. and Huffman, D. R. (1978) Experimental determinations of Mueller scattering matrices for nonspherical particles. *Appl. Opt.* **17,** 2700–2710.

Pradeep, S., Hindelmann, L. M., McMurry, P. H. and Seinfield, J. H. (1995) Organics alter hygroscopic behaviour of atmospheric particles. *J. Geophys. Res.* **100**(D9), 18,755–18,770.

Schichtel, B., Falke, S. R., and Husar, R. B. (1999). North American integrated fine particle data set. CAPITA Report 99-398, p. 15.

Shettle, E. P., and Fenn, R. W. (1979). Models for the aerosols of the lower atmosphere and the effects of humidity variations on their optical properties. Air Force Geophysics Laboratory, Hamscom, Environmental Research Papers, vol. 676, p. 94.

Silva, P. J. and Prather, K. A. (1997) On-line characterization of individual particles from automobile emissions. *Environ. Sci. Technol.* **31,** 3074–3080.

Sloane, C. S. (1983) Optical properties of aerosol: comparison of measurements with model calculations. *Atmos. Environ.* **17**(2), 409–416.
Sloane, C. S. (1984) Optical properties of aerosols of different composition. *Atmos. Environ.* **18**, 871–878.
Sloane, C. S. and Wolff, G. T. (1985) Prediction of ambient light scattering using a physical model responsive to relative humidity: validation with measurement from Detroit. *Atmos. Environ.* **19**(4), 669–675.
Sloane, C. S. (1986) Effects of composition on aerosol light scattering efficiencies. *Atmos. Environ.* **20**(5), 1025–1037.
Sokolik, I. N. and Toon, O. B. (1999) Incorporation of minarological composition into models of the radiative properties of mineral aerosol from UV to IR wavelengths. *J. Geophys. Res.* **104**(D8), 9423–9444.
Stelson, A. W. (1990) Urban aerosol refractive index prediction by partial molar refraction approach. *Environ. Sci. Technol.* **24**(11), 1676–1679.
Tang, I. N., Wong, W. T. and Munkelwitz, H. R. (1981) The relative importance of atmospheric sulphates and nitrates in visibility reduction. *Atmos. Environ.* **15**(12), 2463–2470.
Tang, I. N. and Munkelwitz, H. R. (1994) Water activity, densities, and refractive indices of aqueous sulfates and sodium nitrate droplets of atmospheric importance. *J. Geophys. Res.* **99**(D9), 18,801–18,808.
Tang, I. N. (1996) Chemical and size effects of hygroscopic aerosols on light scattering coefficients. *J. Geophys. Res.* **101**(D14), 19,245–19,250.
Tang, I. N. (1997) Thermodynamic and optical properties of mixed salt aerosols of atmospheric importance. *J. Geophys. Res.* **102**(D2), 1883–1893.
Tang, I. N., Tridico, A. C. and Fung, K. H. (1997) Thermodynamic and optical properties of sea salt aerosols. *J. Geophys. Res.* **102**(D19), 23,269–23,275.
Toon, O. B. (1976) The optical constant of several aerosols species: ammonium sulfate and sodium cloride. *J. Geophys. Res.* **81**, 5733–5748.
Van de Hulst, H.C. (1957). Light Scattering by Small Particles, p. 320. Wiley, New York.
Whitby, K. T. (1977) The physical characteristics of sulfur aerosols. *Atmos. Environ.* **12**, 135–159.
Wilson, R., and Spengler, J. D. (1996). *In Particles in Our Air* (Edited by Wilson, R., Spengler, J. D.). Harvard University Press, Harvard.
World Climate Programme, WCP-55 (1983). *In Report of the Experts Meeting on Aerosols and their Climatic Effects* (Edited by Deepak, A., Gerber, H.E.), p. 107. World Meteorological Organization.